

Attachment Anchors: A Novel Framework for Laparoscopic Grasping Point Prediction in Colorectal Surgery

Dennis N. Schneider, Lars Wagner, Daniel Rueckert, Dirk Wilhelm

Abstract—Accurate grasping point prediction is a key challenge for autonomous tissue manipulation in minimally invasive surgery, particularly in complex and variable procedures such as colorectal interventions. Due to their complexity and prolonged duration, colorectal procedures have been underrepresented in current research. At the same time, they pose a particularly interesting learning environment due to repetitive tissue manipulation, making them a promising entry point for autonomous, machine learning-driven support. Therefore, in this work, we introduce attachment anchors, a structured representation that encodes the local geometric and mechanical relationships between tissue and its anatomical attachments in colorectal surgery. This representation reduces uncertainty in grasping point prediction by normalizing surgical scenes into a consistent local reference frame. We demonstrate that attachment anchors can be predicted from laparoscopic images and incorporated into a grasping framework based on machine learning. Experiments on a dataset of 90 colorectal surgeries demonstrate that attachment anchors improve grasping point prediction compared to image-only baselines. There are particularly strong gains in out-of-distribution settings, including unseen procedures and operating surgeons. These results suggest that attachment anchors are an effective intermediate representation for learning-based tissue manipulation in colorectal surgery.

Index Terms—Perception for Grasping and Manipulation, Surgical Robotics: Laparoscopy, Computer Vision for Medical Robotics, Attachment Anchors

I. INTRODUCTION

MINIMALLY Invasive Surgery (MIS) is a type of surgical intervention in which procedures are performed through small incisions using specialized instruments and intra-abdominal visualization. By limiting tissue trauma, MIS aims to reduce postoperative pain and shorten recovery times, and has therefore largely replaced open surgery in many clinical settings. However, these benefits come at the cost of increased technical complexity and staff workload. MIS is physically and cognitively demanding, especially in colorectal surgery, where procedures are often time-consuming, further exacerbating surgeon fatigue and team workload [1]. Robotic-assisted MIS (RAMIS) promises to alleviate some of these challenges by improving ergonomics, enhancing dexterity, and reducing physiological tremor [2]. Building upon these advantages, further relief may be achieved through the integration of artificial intelligence (AI) and automation into surgical

workflows. Partial automation of repetitive steps or assistance tasks holds the potential to reduce inter-procedure variability as well as reducing cognitive workload [3]. For example, autonomous tissue exposition has been shown to reduce the cumulative activity duration required from surgical assistants [4]. Despite these promising developments, research on AI and automation in surgery has primarily focused on short, highly standardized procedures such as biliary surgery [5], [6]. In contrast, comparatively little attention has been given to more complex procedures such as colorectal surgeries [7], where relevant tissue is more difficult to discern visually, surgical steps are less strictly defined, and intraoperative variability is significantly higher [8]. At the same time, these procedures stand to benefit greatly from AI-driven assistance, for instance through autonomous tissue exposition to support exposure and visualization during prolonged interventions. Considering the high prevalence of colorectal surgery, the limited progress of autonomous surgical robotic assistance in this field indicates a relevant research gap [9].

A promising entry point for addressing this gap lies in focusing on specific surgical phases that are both clinically essential and technically amenable to automation. Colorectal procedures comprise multiple phases with varying complexity and duration. Among these, the colon mobilization phase plays a central role in most colorectal procedures, as the preferred treatment of the majority of colon and rectal cancers requires resection of the tumor-bearing bowel segment together with its supplying vascular pedicle within oncologically safe margins. To enable such resection, the colon and its mesentery must first be sufficiently freed to allow vascular control and subsequent resection. Following removal of the diseased tissue, intestinal continuity is restored by reattaching the remaining bowel ends, referred to clinically as anastomosis. Adequate mobilization is confirmed by the ability to perform a tension-free anastomosis, providing sufficient bowel length for both resection and reconstruction. The colon mobilization phase therefore not only constitutes a crucial preparatory step for the entire procedure and an essential prerequisite for successful colorectal cancer treatment [1], but also a particularly promising entry point for AI-driven robotic assistance.

The article is structured as follows: In Section II, we summarize related work on surgical tissue grasping and exposition that have already been proposed. In Section III, we formalize the task and the proposed problem representation. In Section IV we introduce a machine learning scheme to leverage the attachment anchor knowledge. The results are presented in Section V and discussed in Section VI.

Dennis N. Schneider, Lars Wagner, and Dirk Wilhelm are with the Technical University of Munich, TUM School of Medicine and Health, TUM University Hospital rechts der Isar, Department of Surgery, Research Group MITI, Munich, Germany

Daniel Rueckert is with the Technical University of Munich, TUM School of Medicine and Health, TUM University Hospital rechts der Isar, Chair for AI in Healthcare and Medicine Munich, Munich, Germany and with the Department of Computing, Imperial College London, London, UK

II. RELATED WORK

The fundamental objective of robotic manipulation is to enable interaction with the environment through actions such as grasping and object handling. In conventional robotic manipulation, this is typically formulated as estimating feasible six-degrees-of-freedom grasping poses for rigid objects using visual and depth information, as described in [10]–[13]. These approaches usually leverage either a priori knowledge of the expected 3D models being mapped onto the perceived point clouds or learn the grasping task directly from the point clouds [14].

The objective for laparoscopic surgical grasping differs fundamentally from that of conventional robotic manipulation due to the constraints imposed by the surgical environment. Most notably, laparoscopic instruments are inserted through a fixed insertion point, restricting the available degrees of freedom. Consequently, the reachable workspace and admissible orientations are largely constrained through the pivot point [15], and rotation along the tool-axis being mostly dependent on the local surface-normal. Thus, laparoscopic grasping approaches generally focus on predicting suitable grasping points rather than estimating full six-degree-of-freedom grasp poses [5], [16].

Unlike non-surgical grasping scenarios, the surgical domain generally lacks prior knowledge in the form of accurate 3D models of the graspable structures. Some approaches therefore rely on aligning generated candidate organs to observed point-clouds [5], a process that can require substantial computational effort with runtimes up to 60 seconds. Other approaches avoid this overhead by inferring grasping points directly from local depth information [16], [17]. Moreover, the deformable nature of biological tissue complicates surgical grasping tasks. Rather than single pick-and-place action, surgical tissue manipulation can be broken down into two separate tasks: (1) identifying a suitable grasping point for a certain surgical action and (2) executing the tissue exposition trajectory that deforms the tissue in a controlled manner while avoiding rupture or damage to surrounding structures. Most current research focuses on the latter, often formulating the problem using Lagrangian-based mechanical principles to compute optimal exposition trajectory given a fixed grasping point [18], [19]. Thereby, an additional challenge is the interconnectedness of anatomical structures. Both grasping points and exposition trajectories depend on an understanding of tissue attachments to prevent excessive strain or tearing. To address this issue, previous research have introduced the concept of attachment points, which use structured representations, such as grids, to model connections between adjacent tissues [18], [20], [21].

However, most related work [16], [17], [20], [21] makes use of simplified scenarios to evaluate their approaches, which may not fully capture the complexity of real surgical environments in terms of anatomical topology and visual appearance. Approaches validated in more realistic settings are often limited to relatively standardized procedures, such as cholecystectomy [5], [6], in which visually distinct structures, like the liver and gallbladder, simplify intraoperative perception. In contrast, comparatively little research has addressed

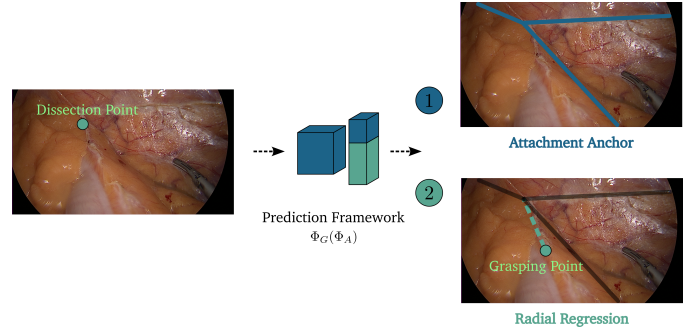


Fig. 1. Pipeline of the proposed grasping point prediction framework. The model first detects and classifies the attachment anchor representation from the input image and then predicts a grasping point relative to the anchor origin.

colorectal surgery [22], [23], where tissue appearance is less distinctive and procedural variability is higher. Therefore, in this work, we address the problem of grasping point prediction for deformable tissue as a first step towards autonomous tissue manipulation in colorectal surgery. To this end, we propose a novel visual representation called *attachment anchors* that explicitly incorporates tissue attachment information and mechanical constraints into a simplified model (see Fig. 1). This condensed representation eliminates the need for precise semantic segmentation, making the approach better suited to the visually complex and highly variable environments encountered in colorectal procedures. The model statistically reduces the complexity of the surgical grasping problem, enabling more robust grasping point prediction under realistic conditions. The main contributions of this paper are:

- We propose *attachment anchors*, a novel visual representation for surgical grasping point prediction during the colorectal colon mobilization phase.
- We present a grasping point prediction framework based on attachment anchors and radial regression and statistically validate its applicability on real-world colorectal surgical cases.
- We demonstrate that the proposed representation outperforms image-only baselines in visual tissue manipulation prediction and enables realistic, task-relevant data augmentations.

III. PROBLEM ANALYSIS

In Section III-A, we first formalize the task of surgical grasping point prediction. Section III-B then introduces attachment anchors as a novel surgical scene representation using three representative retraction cases.

A. Task Formulation

Let a surgical site be given by a set of interconnected tissue and organs, which the surgeon aims to separate in the course of a surgery. Separation of organs is achieved by the principle of dissection, which means the repetitive and sequential transection of connecting tissue. For one single step this can be formulated as the dissection of a point D located on the surgical site. To achieve this task, the surgeon exposes this region by grasping the respective organ at a suitable point G

and gently applying a retraction motion in a suitable direction. The retraction motion can accordingly be seen as a solution to the problem of exposing a certain dissection point. Thus, from a modeling perspective, tissue exposition can be described as selecting a grasping point G and direction that enable sufficient visualization of the queried dissection point D . In clinical practice, this selection is based solely on the tissue’s visual appearance and the surgeon’s implicit understanding of the underlying mechanical constraints and tissue connectivity.

With this understanding surgeons classify the surgical site into different anatomical segments. Our approach aims to reproduce this abstracted scene understanding by formulating the task of grasping point prediction. Given an intraoperative image I of the surgical site and a specified dissection point D , the task is to predict an appropriate grasping point G on the visible tissue. Formally, we seek to learn a mapping

$$f_{\Phi} : (I, D) \mapsto G, \quad (1)$$

where f_{Φ} denotes a parameterized model that infers grasping points from visual input alone. We evaluate our proposed model by comparing the predicted grasping points to those selected by expert surgeons in identical visual situations. The degree to which the model reproduces the surgeons’ chosen grasp locations indicates how well it captures the underlying tissue topology and the visual-mechanical reasoning required for effective tissue manipulation.

B. Case Discrimination

For accurate grasping point prediction, we introduce the attachment anchor framework (see Fig. 1), which provides an abstract representation of the local mechanical configuration relevant to a grasping maneuver. Formally, an attachment anchor is defined in a two-dimensional polar coordinate system around its mechanical origin O . Directions are represented on the unit circle \mathbb{S}^1 , allowing angular relationships to be modeled independently of scale. Each attachment anchor consists of the mechanical center O and three directed unit vectors originating from there; two mounting vectors $\mathbf{e}_{mnt,1}$ and $\mathbf{e}_{mnt,2}$ representing attachments of the tissue to rigid or semi-rigid anatomical structures, and one adhesion vector \mathbf{e}_{adh} encoding the dominant direction of tissue adherence. When vectors share the same semantic role, they are indexed in clockwise order.

We consider a surgical scene during the colon mobilization phase, where the primary tissue components include the colon, surrounding connective tissue, and the abdominal wall. As the objective of colon mobilization is to separate the colon and its mesentery from its rigid anatomical attachments, we abstract the scene into two interacting elements, the deformable tissue to be mobilized and its rigid mounting. Based on this abstraction, we can distinguish three general retraction cases (see Fig. 2).

Case 1: Adhesion strand. A single, narrow adhesion strand connects the deformable tissue to the rigid mounting, with the dissection point D located on the adhesion itself (see Fig. 2a). To generate linear tension along the strand, the grasping point G is selected along its linear extension. The adhesion is represented by a unit vector \mathbf{e}_{adh} aligned with the

strand’s centerline and originating at the visually identifiable attachment point O on the rigid mounting farthest from the deformable tissue. The rigid mounting is encoded by the two unit vectors $\mathbf{e}_{mnt,1}$ and $\mathbf{e}_{mnt,2}$, capturing its orientation and perspective. While the adhesion vector specifies the location and orientation of the adhesion, the enclosed region \mathcal{R}_{mnt} spanned by the mounting vectors represents the visible features of the rigid mounting region.

Case 2: Adhesion triangle. A wide adhesion remains attached to the rigid mounting on one side while being detached on the other (see Fig. 2b). This configuration commonly arises during partial mobilization as dissection progresses along the mounting. The dissection point D is located along the remaining attachment between the adhesion and the rigid structure, indicating that dissection should continue at this interface. The corresponding grasping point G applies tension at D by grasping the deformable tissue and inducing a rotational retraction motion. This widens the dissected angle in a hinge-like manner. The adhesion triangle is modeled as a mechanical hinge between the attached soft tissue and the tissue that has already been dissected. The hinge location is defined at the intersection of both attachment states. A unit vector \mathbf{e}_{adh} follows the detached edge of the adhesion tangentially and represents the direction in which the hinge opens. Two mounting vectors, $\mathbf{e}_{mnt,1}$ and $\mathbf{e}_{mnt,2}$, encode the current and former attachment to the rigid mounting, respectively. This gives rise to the triangular shape of the deformable tissue. Beyond their mechanical interpretation, the vectors enclose regions with distinct semantic and visual characteristics. Region \mathcal{R}_{adh} between \mathbf{e}_{adh} and $\mathbf{e}_{mnt,1}$ corresponds to the manipulable soft tissue. Region \mathcal{R}_{mnt} between $\mathbf{e}_{mnt,1}$ and $\mathbf{e}_{mnt,2}$ captures the rigid mounting which is of notably different texture and coloring. Region \mathcal{R}_{diss} between $\mathbf{e}_{mnt,2}$ and \mathbf{e}_{adh} captures the open hinge, which is visually distinct due to its marks from previous dissection. It also represents the semantic meaning of opening up for target fulfillment.

Case 3: Plane adhesion. A plane adhesion is fully attached to the rigid mounting over a wide contact area (Fig. 2c), resulting in grasping and manipulation forces being distributed relatively evenly along the attachment. Consequently, feasible grasping points G are less localized, as similar retraction effects can be achieved from a broader range of locations. The surgical objective in this configuration is to pull the adhesion away from the mounting to generate tension along the entire boundary between soft tissue and rigid structure, thereby facilitating continuous dissection along this interface. The plane adhesion is represented by the local boundary separating deformable tissue from the rigid mounting. As this boundary alone does not define a unique anchor location, the attachment anchor is defined at the boundary point closest to the dissection point D , ensuring an unambiguous reference. Consistent with Case 2, two vectors $\mathbf{e}_{mnt,1}$ and $\mathbf{e}_{mnt,2}$ are defined tangentially along the boundary to encode the rigid mounting, while the adhesion vector \mathbf{e}_{adh} points toward the deformable tissue, distinguishing it from the mounting. This formulation yields a simplified yet expressive representation of plane adhesions, capturing the distinct mechanical, semantic, and visual characteristics associated with each vector and

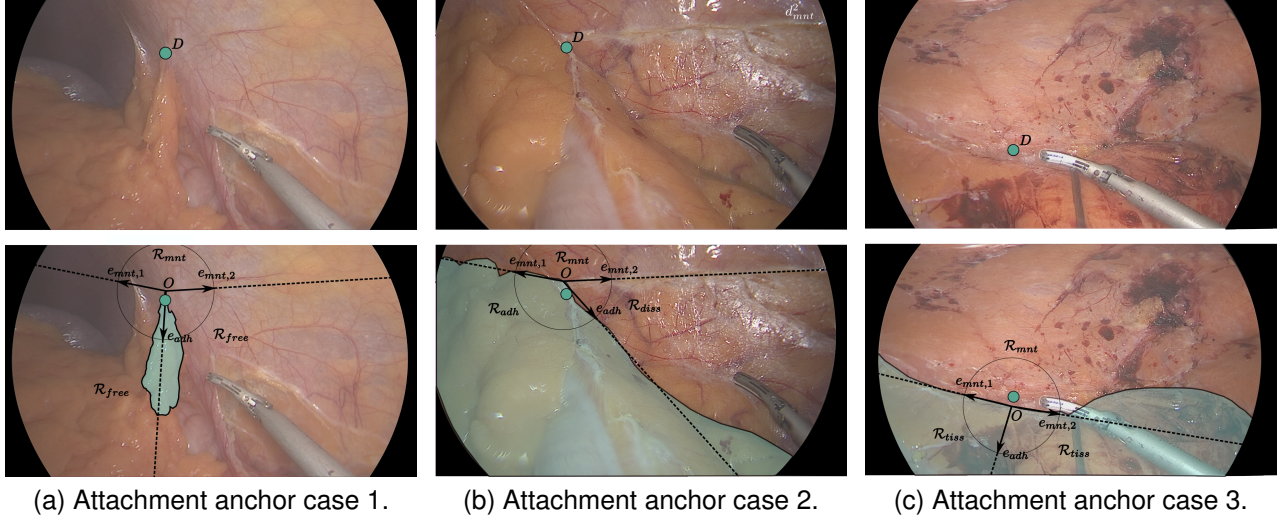


Fig. 2. Example surgical input images illustrating the three attachment anchor cases. Each image shows the dissection point D (top) and the corresponding attachment anchor representation (bottom), with the soft tissue of interest highlighted in blue.

enclosed region.

IV. METHODOLOGY

In Section IV-A, we first describe the attachment anchor encoder, which extracts a structured anchor representation from an input image and query dissection point. In Section IV-B, we then present the task-specific grasping-point decoder that predicts grasp locations based on the learned attachment topology. Finally in Section IV-C, we describe the dataset used for training and evaluation.

A. Attachment Anchor Encoder

The attachment anchor representation A of an image I and dissection target D is obtained by passing it through our

attachment anchor encoder Φ_A :

$$A = \Phi_A(I, D). \quad (2)$$

The encoder Φ_A is implemented as a YOLOv8-based [24] object detection architecture with a *MobileNetV3-small* [25] backbone. To balance spatial resolution and semantic richness, we extract intermediate feature maps from layer *blocks.3*, which serve as the basis for medium-resolution feature learning. A YOLO-style detection head is appended for attachment anchor prediction. This head performs keypoint-based detection, identifying both the mechanical center O of an attachment anchor and its three defining directional vectors \mathbf{e}_{adh} , $\mathbf{e}_{mnt,1}$, and $\mathbf{e}_{mnt,2}$. To account for the different anchor configurations introduced in Section III-B, we employ one prediction head per anchor type. A discrete gate $o_{gate} \in \{0, 1, 2\}$ classifies the responsible head for each activated grid cell. Each prediction head outputs a center-offset $c \in [-1, 1]^2$, localizing the respective attachment anchor within the activated grid cell, along with three two-dimensional anchor-vectors $\mathbf{e}_i \in [0, 1]^2$, $i \in 0, 1, 2$, encoding the orientation of the attachment anchor.

To ensure consistent feature representations across semantically similar regions, we further leverage the intermediate feature maps for contrastive representation learning at medium resolution. Specifically, we apply an InfoNCE-Loss [26] to enforce similarity between feature embeddings corresponding to regions with equivalent semantic meaning. We consider regions \mathcal{R}_{mnt} as semantically equivalent throughout all cases, as they consistently represent the rigid abdominal wall irrespective of the specific retraction configuration. Likewise, multiple occurring regions \mathcal{R}_{free} (and \mathcal{R}_{tiss}) are treated as semantically equivalent, reflecting symmetry in configurations where multiple “free” or “tissue” regions fulfill the same functional role. The attachment encoder pipeline is shown in Fig. 3.

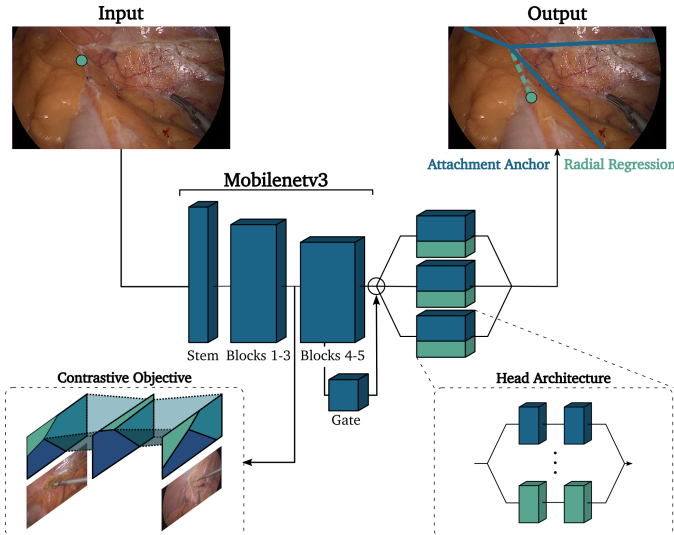


Fig. 3. Architecture of the proposed model. The attachment anchor encoder ϕ_A (blue) extracts the anchor representation, which is then used by the grasping point decoder ϕ_G (cyan).

B. Grasping Point Decoder

The learned attachment anchor representation A is subsequently leveraged to predict the grasping point. To this end, we introduce a grasping point detection decoder Φ_G , which extends on the pretrained attachment prediction head with situation-aware grasping point regression. Given an attachment anchor representation A encoded by Φ_A , the decoder Φ_G predicts the grasping point in a local, anchor-centric coordinate system. Specifically, the grasping location is parameterized in polar coordinates relative to the predicted anchor center. The decoder regresses an offset direction

$$\phi_{rel} \in \mathbb{R}^2, \quad \|\phi_{rel}\|_2 = 1, \quad (3)$$

which represents a unit direction vector on the unit circle and is defined relative to the adhesion direction α_{adh} of the corresponding vector e_{adh} . This formulation enforces rotational consistency between the anchor orientation and the predicted grasp direction. In addition, the decoder predicts a relative radial distance $r_{rel} \in [0, 1]$ obtained via a sigmoid activation and scaled by the diagonal length of the input image, thereby yielding the final grasping point location

$$G = A_{center} + r_{rel} \cdot \text{diag}(I) \cdot \phi_{rel} \quad (4)$$

By conditioning grasp prediction on anchor position, orientation, and anchor type, the decoder enables situation-aware grasping, with each anchor-specific prediction head learning a distinct solution manifold tailored to its corresponding retraction case. The resulting architecture, consisting of the anchor-pretrained encoder Φ_A and the task-specific grasp decoder Φ_G with radial regression, is referred to as *Rad-YOLOv8*.

C. Dataset

For learning the encoder Φ_A and decoder Φ_G , we use a self-curated in-house dataset of laparoscopic colorectal surgeries. The dataset comprises 90 colorectal surgical interventions collected at the TUM University Hospital between 2015 and 2025. Data collection was conducted under ethical approval from the Ethics Committee of the TUM University Hospital (approval number: 337/21 S), and written informed consent was obtained from all patients. The dataset consists of laparoscopic colorectal procedures spanning five anatomical subregions along the colon, as illustrated in Fig. 4. Specifically, ileocecal resections involve mobilization and removal of the terminal ileum and cecum. Right hemicolectomies extend this resection to the ascending colon and hepatic flexure, while left hemicolectomies address the descending colon and splenic flexure. Sigmoid resections focus on the mobilization and removal of the sigmoid colon, and rectal resections entail deep pelvic dissection of the rectum. In addition, the dataset contains three proctocolectomies, in which the entire colon is resected.

The surgeries were performed by 15 different surgeons with diverse clinical backgrounds, resulting in a dataset reflecting a wide range of operative styles and anatomical variability. As mentioned in Section I, colon mobilization is a critical component to all included colorectal procedures. Therefore, the dataset is restricted to grasping maneuvers occurring during

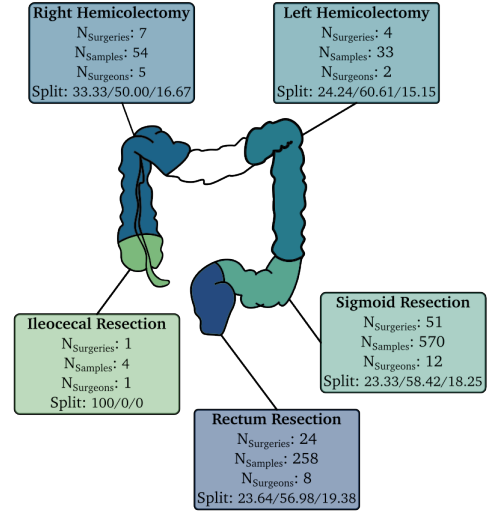


Fig. 4. Dataset composition showing colorectal surgical procedures stratified by anatomical region along the colon.

the colon mobilization phase. Nevertheless, this scope covers a considerable amount of anatomical diversity. The dataset consists of image samples to individual grasping maneuvers, each extracted at the time point immediately preceding tissue grasping, where the surgeon has an unobstructed view of the intended dissection target.

D. Evaluation Metrics

Model performance is evaluated in terms of grasping point prediction using *Precision@6%*. A prediction is considered correct if it lies within a circular region centered on the ground-truth grasping point. Given the 7×7 output grid of the YOLO backbone, the radius of this region is set to one-seventh of the image size. This corresponds to a positive area covering approximately 6.4% of the input image. Since non-maximum suppression yields a single grasp prediction for most samples, recall and F1-score are omitted because they do not differ significantly across models.

To evaluate the effectiveness of the proposed attachment anchor framework, we compare various model variants by ablating the information provided by attachment anchors. As a baseline, we use a standard YOLOv8 architecture adapted for keypoint detection. This architecture directly predicts grasping points from images without any anchor-based representation (KP-YOLOv8), following the setup described in Section IV-A. A second variant incorporates attachment anchors as an auxiliary pretraining objective while retaining the same prediction formulation (Abs-YOLOv8). Finally, we evaluate the full proposed architecture, which explicitly leverages the attachment anchor representation and employs radial regression for relative grasping point prediction (Rad-YOLOv8).

V. EXPERIMENTS AND RESULTS

In this section, we evaluate the impact of attachment anchors on surgical grasping point prediction. In Section V-A, we first demonstrate the statistical simplification on the grasping

problem enabled by the attachment anchor framework and analyze the predictability of the attachment anchors from surgical images (Section V-B). We then assess their effect on the grasping point prediction task using attachment anchor knowledge (Section V-C), followed by generalization studies on unseen surgeries (Section V-D) and unseen surgeons (Section V-E). Finally, we examine realistic data augmentations enabled by the attachment anchor framework in Section V-F.

A. Statistical Analysis

We analyze the effect of attachment anchors on the grasping task by examining the spatial distributions of grasping and dissection points normalized to the attachment anchor representation (Fig. 5). All samples are grouped by attachment anchor case and superimposed after a normalization procedure aligns the anchors to a common reference frame. Specifically, each anchor is translated to a shared origin while its defining vectors are warped to fixed orientations. Vectors $\mathbf{e}_{mnt,1}$ and $\mathbf{e}_{mnt,2}$ are aligned horizontally. Vector \mathbf{e}_{adh} is normalized vertically downward. This warping transformation keeps ratios between the anchor directions and radial distance to the attachment anchor’s center intact.

Table I reports the standard deviations of the resulting distributions of the absolute grasping points (*Absolute*), grasping points expressed relative to their dissection targets (*Relative*), and grasping points after attachment anchor-based normalization. Across all cases, anchor normalization yields a statistically significant reduction in standard deviation along the x-axis in a one-sided pairwise t-test between relative and attachment anchor-normalized representation. Due to the distribution of samples along the y-axis, the standard deviation in x-axis is the relevant deviation axis to consider and showcases a significant explanation of uncertainty by the proposed model.

A closer inspection of the normalized distributions in Fig. 5 reveals case-specific patterns. In case 1, dissection points are tightly clustered below the anchor center along the adhesion direction \mathbf{e}_{adh} , reflecting the mechanical origin of the adhesion. Correspondingly, grasping points form a linear extension along the same direction. Case 2, which is inherently asymmetric, is normalized such that region \mathcal{R}_{adh} lies in the lower-left quadrant. Dissection points concentrate along \mathbf{e}_{adh} and $\mathbf{e}_{mnt,1}$, consistent with continued dissection along the remaining adhesion, while grasping points predominantly lie within \mathcal{R}_{adh} near \mathbf{e}_{adh} to maintain exposure of the dissection target. In case 3, dissection points tend to cluster near the boundary between soft tissue and mounting, whereas grasping points exhibit substantially higher variability. This reflects the evenly distributed attachment of plane adhesions, where multiple grasping points yield similar tissue responses. This leads surgeons to prioritize ergonomic considerations. Accordingly, case 3 exhibits the highest x-axis standard deviation in Table I.

B. Attachment Anchor Prediction

We next assess the quality of attachment anchor prediction from an input image I and dissection point D . Quantitative

TABLE I
STANDARD DEVIATIONS OF GRASPING AND DISSECTION POINT DISTRIBUTIONS ACROSS ABSOLUTE COORDINATES, RELATIVE-TO-DISSECTION COORDINATES, AND ATTACHMENT ANCHOR-BASED NORMALIZED REPRESENTATIONS.

Type	Grasp		Dissect	
	std(x) (%)	std(y) (%)	std(x) (%)	std(y) (%)
<i>Absolute</i>	17.81	17.09	16.45	17.22
Case 1	18.29	16.91	17.54	16.19
Case 2	16.87	17.11	15.32	17.01
Case 3	18.05	17.41	17.27	16.24
<i>Relative</i>	13.53	15.74	-	-
Case 1	11.77	14.03	-	-
Case 2	13.19	15.94	-	-
Case 3	15.52	14.51	-	-
<i>Attachment Anchors</i>				
Case 1	8.57*	15.69	1.40	8.03
Case 2	10.08†	16.44	4.63	14.27
Case 3	11.66†	12.85	1.16	4.24

(one-sided pairwise t-test)

† p < 0.01

* p < 0.05

results are reported in Table II, obtained using 5-fold cross-validation with folds balanced with respect to attachment anchor case distribution and total sample count.

Incorporating attachment anchor knowledge through contrastive feature learning leads to a substantial improvement in localization performance. Specifically, Precision@6% increases by 9.60% accompanied by a marked reduction in localization error, indicating more accurate anchor center prediction. Anchor directions also benefit from the contrastive objective as reported in Table III. In contrast, the prediction accuracy of the anchor type improves only marginally, suggesting that the primary benefit of the contrastive objective lies in learning a more discriminative spatial representation rather than enhanced categorical discrimination.

TABLE II
ATTACHMENT ANCHOR PREDICTION PERFORMANCE (MEAN ± STANDARD DEVIATION %) UNDER 5-FOLD CROSS-VALIDATION. RESULTS COMPARE A PURELY IMAGE-BASED KEYPOINT DETECTOR (KP-YOLOv8) WITH THE SAME ARCHITECTURE AUGMENTED BY CONTRASTIVE LEARNING.

Model	Precision@6% ↑	RMSE ↓	Type Precision ↑
KP-YOLOv8	78.24 ± 2.62	12.91 ± 4.81	64.50 ± 5.64
+ Contrastive	87.84 ± 3.40†	9.75 ± 1.66	67.17 ± 7.84

† p < 0.01

* p < 0.05

C. Experiments Using Attachment Anchors

We next evaluate the impact of attachment anchor representations on the grasping point prediction task. Prediction performance is compared across the proposed model variants using 5-fold cross-validation with evenly distributed splits, following the same protocol as in Section V-B. Quantitative results are summarized in Table IV.

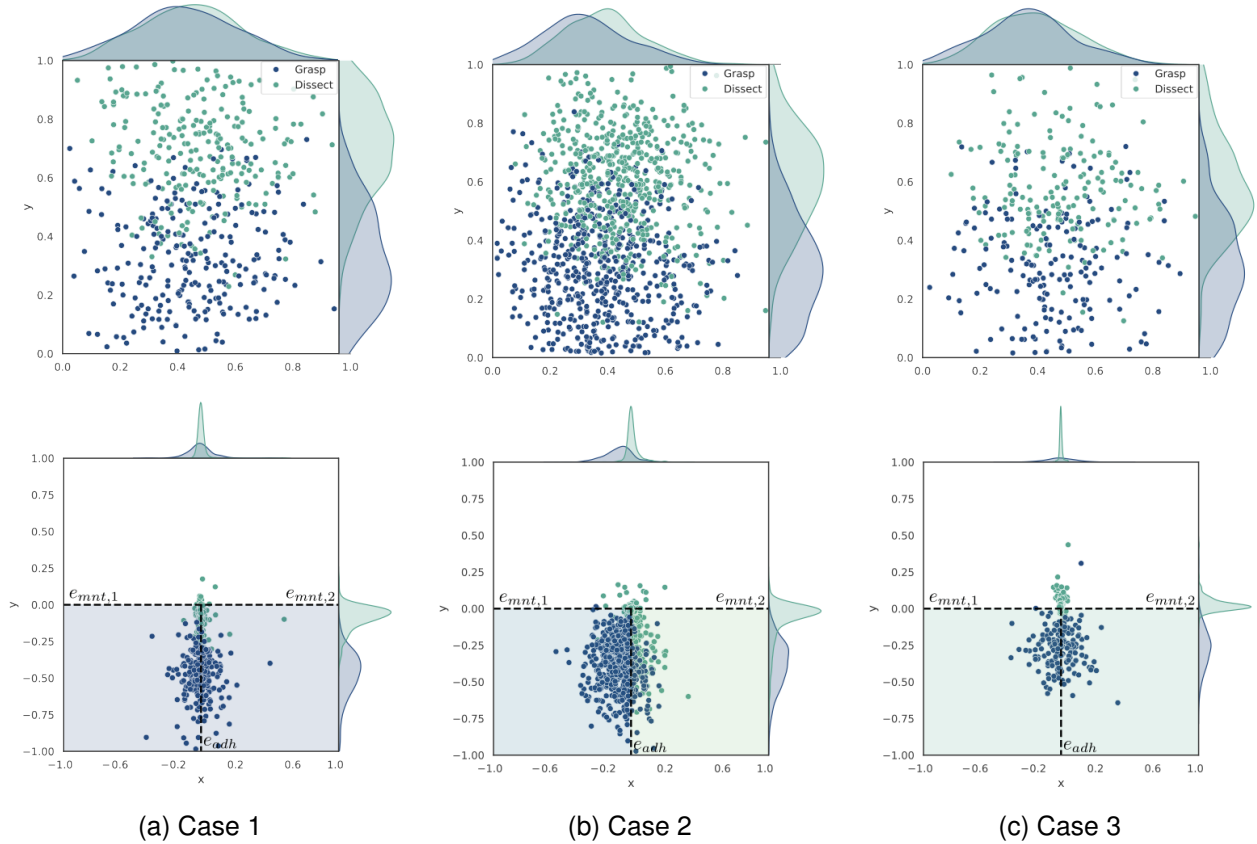


Fig. 5. Statistical distribution of grasping points before and after normalizing with attachment anchors, per case.

TABLE III
ATTACHMENT ANCHOR DIRECTION PREDICTION PERFORMANCE (MEAN RMSE \pm STANDARD DEVIATION *radian*) UNDER 5-FOLD CROSS-VALIDATION. RESULTS COMPARE A PURELY IMAGE-BASED KEYPOINT DETECTOR (KP-YOLOv8) WITH THE SAME ARCHITECTURE AUGMENTED BY CONTRASTIVE LEARNING.

Model	RMSE (rad) \downarrow		
	e_{adh}	$e_{mnt,1}$	$e_{mnt,2}$
KP-YOLOv8	0.55 ± 0.04	0.63 ± 0.04	0.65 ± 0.09
+ Contrastive	$0.48 \pm 0.03^*$	$0.57 \pm 0.04^*$	0.60 ± 0.04

$\dagger p < 0.01$

* $p < 0.05$

TABLE IV
GRASPING POINT PREDICTION PERFORMANCE (MEAN \pm STANDARD DEVIATION %) UNDER 5-FOLD CROSS-VALIDATION. RESULTS COMPARE VISION-ONLY PREDICTION WITH MODELS INCORPORATING ATTACHMENT ANCHOR REPRESENTATIONS.

Model	Precision@6% \uparrow	RMSE \downarrow
<i>Vision only</i>		
KP-YOLOv8	37.80 ± 2.44	18.63 ± 0.84
<i>Attachment Anchors</i>		
Abs-YOLOv8	49.90 ± 4.60	$14.77 \pm 1.12^\dagger$
Rad-YOLOv8	$51.20 \pm 3.70^\dagger$	15.00 ± 1.44

$\dagger p < 0.01$

* $p < 0.05$

Incorporating attachment anchor information yields a substantial and statistically significant improvement in grasp localization performance. Compared to the vision-only baseline (KP-YOLOv8), the inclusion of attachment anchor pretraining (Abs-YOLOv8) increases Precision@6% by 12.10%, while also reducing localization error as measured by RMSE. Adding an explicit radial grasping representation to the model (Rad-YOLOv8) results in a slight increase of 1.30% in Precision@6%. However, this improvement is not statistically significant. This suggests that the primary performance gain stems from the attachment anchor representation itself rather than from the specific grasp parameterization.

D. Generalization to Unseen Surgeries

We evaluate the ability of the proposed approach to generalize to previously unseen surgeries, thereby assessing its robustness to novel anatomical and visual configurations. In this setting, both attachment anchor prediction and subsequent grasping-point prediction are evaluated exclusively on surgeries not observed during training. This evaluation is particularly challenging, as the dataset spans multiple anatomical subregions of the colon (see Fig. 4), each exhibiting distinct visual appearances and tissue configurations.

Quantitative results are reported in Table V. Incorporating attachment anchor representations substantially improves per-

TABLE V
GRASPING POINT PREDICTION PERFORMANCE (MEAN \pm STANDARD DEVIATION %) ON UNSEEN SURGERIES ACROSS 5 EVALUATION RUNS.

Model	Precision@6% on unseen surgery type \uparrow				Mean (%)
	Sigmoid	Rectum	Hemicol. left	Hemicol. right	
KP-YOLOv8	30.66 \pm 2.77	41.60 \pm 3.01	27.04 \pm 4.32	33.89 \pm 10.26	33.30
Abs-YOLOv8	43.39 \pm 1.04	52.06 \pm 1.86	36.30 \pm 1.48\dagger	50.33 \pm 4.90*	45.52
Rad-YOLOv8	44.10 \pm 1.54\dagger	52.22 \pm 1.65\dagger	35.40 \pm 2.44	48.85 \pm 4.45	45.14

\dagger $p < 0.01$

* $p < 0.05$

formance across all unseen surgical categories. Notably, the largest performance gain of 16.44% is observed for right hemicolectomy procedures, where the vision-only baseline struggles due to pronounced visual and anatomical differences compared to the training data. In contrast, left hemicolectomy procedures exhibit a smaller but still significant improvement of 9.26%, which can be attributed to their greater anatomical similarity to sigmoid resections encountered during training.

Overall, attachment anchors consistently enhance generalization performance across all surgical types, with statistically significant improvements in every surgical procedure ($p \leq 0.012$, unpaired t-test). These results indicate that the proposed representation captures scene-level structural information that is transferable across diverse colorectal surgical procedures.

E. Generalization to Unseen Surgeons

The dataset comprises grasping actions recorded during routine clinical practice. This introduces inevitable surgeon-specific biases because only one grasping action is annotated as correct for each situation. To assess the extent to which the proposed model generalizes beyond individual ergonomic preferences, we evaluate performance on previously unseen operating surgeons.

Due to an imbalance in the number of samples per surgeon, surgeons are grouped to ensure that each group accounts for at least 15% of the dataset, enabling statistically meaningful evaluation. Generalization across surgeon groups provides insight into whether the model captures task-relevant grasping principles rather than overfitting to individual grasping styles. Quantitative results are reported in Table VI.

Without attachment anchor representations, the vision-only baseline exhibits limited generalization to unseen surgeons, achieving a mean Precision@6% of 37.76%. Incorporating attachment anchors substantially improves robustness, increasing mean precision to 50.14%. The radial grasping formulation yields comparable performance (49.95%), indicating that the primary gain stems from the anchor-based scene representation rather than the specific grasp parameterization.

F. Experiments on Emerging Transformations

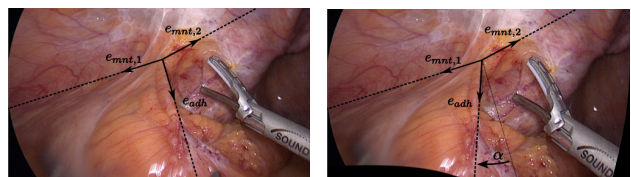
Introducing attachment anchors as a means of partitioning the scene into distinct semantic regions enables novel, anatomically meaningful data transformations. In this experiment, we evaluate anchor-derived warp transformations and analyze their impact on grasping point prediction performance.

The attachment anchor representation allows for the controlled manipulation of specific scene components while preserving overall anatomical plausibility. In particular, we generate realistic variations of the surgical scene by warping only the adhesion direction vector e_{adh} , thereby locally extending or compressing the angular configuration of the surrounding image regions. Let R denote a planar rotation matrix. The warped adhesion vector is defined as

$$e_{adh}^{(warp)} = R(\alpha)e_{adh} \quad \alpha \sim \mathcal{U}\left(\left[-\frac{\pi}{18}, \frac{\pi}{18}\right]\right). \quad (5)$$

As illustrated in Fig 6, this transformation produces subtle yet realistic deformations of the adhesion, while leaving unrelated regions of the scene unaffected. The induced variation predominantly influences grasping positions farther from the anchor center O , thereby encouraging the model to better capture the spatial extent and orientation of relevant anatomical structures.

Quantitative results are reported in Table VII. Incorporating anchor-based warp transformations consistently improves grasping point prediction performance for both attachment-anchor-based models. This demonstrates that the proposed representation not only simplifies the grasping task but also enables realistic and effective data augmentation strategies tailored to the surgical domain.



(a) Before Transformation. (b) After Transformation.

Fig. 6. Example of a realistic surgical scene transformation obtained by warping only the adhesion vector e_{adh} .

VI. DISCUSSION

In this work, we introduced attachment anchors as a compact, interpretable representation of surgical scenes that encodes mechanical, visual, and semantic information relevant to tissue manipulation. By abstracting local tissue-mounting relationships into a small set of geometrically defined primitives, attachment anchors offer a simplified yet expressive description of situations relevant to grasping during colorectal surgery.

Our results demonstrate that this representation significantly reduces uncertainty for the task of surgical grasping point

TABLE VI
GRASPING POINT PREDICTION PERFORMANCE (MEAN \pm STANDARD DEVIATION %) ON UNSEEN SURGEONS ACROSS 5 EVALUATION RUNS. SURGEONS ARE GROUPED TO ENSURE SUFFICIENT SAMPLE SIZES PER GROUP.

Model	Precision@6% on unseen surgeon identifier \uparrow						Mean (%)
	1	2	3	4, 5, 6	7, 8, 9	10, 11, 12, 13, 14	
KP-YOLOv8	43.05 \pm 2.76	34.71 \pm 2.00	43.56 \pm 5.35	33.25 \pm 5.22	33.72 \pm 2.65	38.28 \pm 6.67	37.76
Abs-YOLOv8	56.27 \pm 3.62[†]	38.82 \pm 2.73	53.97 \pm 1.49[†]	53.18 \pm 3.97	48.57 \pm 1.43[†]	50.00 \pm 3.45[†]	50.14
Rad-YOLOv8	55.17 \pm 4.74	40.68 \pm 3.50*	51.77 \pm 1.32	55.82 \pm 4.59[†]	48.20 \pm 3.35	48.05 \pm 2.71	49.95

[†] $p < 0.01$

* $p < 0.05$

prediction. Assuming perfect attachment anchor prediction, we show that the grasping problem becomes substantially more constrained. This highlights the theoretical relevance of attachment anchors as an intermediate representation. Furthermore, we demonstrate that attachment anchors can be reliably predicted from surgical images, and their inclusion improves the prediction of grasping points.

A central finding of this work is that attachment anchors enable strong generalization capabilities. These performance gains are particularly pronounced in slightly out-of-distribution settings, such as unseen surgical procedures with distinct anatomical characteristics. For instance, in left and right hemicolectomies, where the visual appearance differs greatly due to the presence of structures like the liver, attachment anchors notably enhance robustness (see Table V). These results suggest that the proposed representation effectively mitigates uncertainty arising from anatomical variability by focusing on local, mechanically grounded scene structure rather than global appearance.

The improvement observed in generalization to unseen surgeons further supports the idea that attachment anchors capture grasping principles driven by the task rather than surgeon-specific ergonomic preferences (see Table VI).

Beyond improving performance and generalization in grasping point prediction, attachment anchors offer important conceptual advantages for autonomous RAMIS. They provide an explicit explanation of how the model perceives grasping-relevant situations and offer a local and interpretable representation of them. This interpretability is particularly valuable in safety-critical domains, such as surgery. If the predicted attachment anchor accurately reflects the situation, then the likelihood of a correct grasping point prediction is high. Erroneous anchor predictions can also be identified and inspected, which is a first step toward explainable and verifiable

autonomous surgical assistance.

Although attachment anchors offer an effective representation of situations relevant to grasping, their applicability is subject to several practical limitations. The dataset used in this study has inherent biases, such as imbalances among surgeons and procedures, and a significant central bias in grasping and dissection point locations caused by laparoscopic camera operation (see Figure 7). Although these effects are mitigated through careful experimental design and statistical evaluation, they nevertheless limit the diversity of observed scenarios. In addition, the analysis is restricted to samples in which both the grasping and dissection points are visible. This reduces the size of the available dataset and excludes situations with partial occlusions. Extending the framework to handle hidden or temporally inferred targets is a promising direction for future work. Furthermore, the statistical analysis relies on a simplified scene abstraction. Deviations observed outside the adhesion region, \mathcal{R}_{adh} , reflect the limited expressiveness of a single attachment anchor when describing complex tissue configurations at larger distances. Nevertheless, this simplicity is also a key strength of the proposed representation. By relying on local geometric and mechanical cues, the attachment anchors avoid the complexity specific to surgery and naturally recur across different procedures and anatomical regions. For a given dissection target D , the relevant attachment anchor is usually located nearby and characterized by straightforward geometric relationships, which explains why it is applicable in so many different surgical contexts.

Future work may investigate the robustness of attachment anchors under more challenging conditions encountered in RAMIS, including extensive bleeding or fogging and cross-center surgeons and instrumentation. Furthermore, the general nature of the proposed representation suggests its applicability to other robotic procedures that rely on tissue mobilization and retraction beyond colorectal surgery.

TABLE VII
GRASPING POINT PREDICTION PERFORMANCE (MEAN \pm STANDARD DEVIATION %) WITH AND WITHOUT ATTACHMENT ANCHOR-BASED WARP TRANSFORMATIONS, EVALUATED OVER 5 INDEPENDENT RUNS.

Model	Precision@6% \uparrow	
	W/o augmentation	With augmentation
Abs-YOLOv8	49.90 \pm 4.60	52.27 \pm 3.93
Rad-YOLOv8	51.20 \pm 3.70	52.55 \pm 3.05

A. Conclusion

In summary, this study shows that attachment anchors provide a concise and understandable representation of surgical scenes and are an effective intermediate representation for learning-based tissue manipulation. By combining mechanical, visual, and semantic information, attachment anchors reduce uncertainty in predicting grasping points and can be reliably inferred from image data. Experimental results show consistent

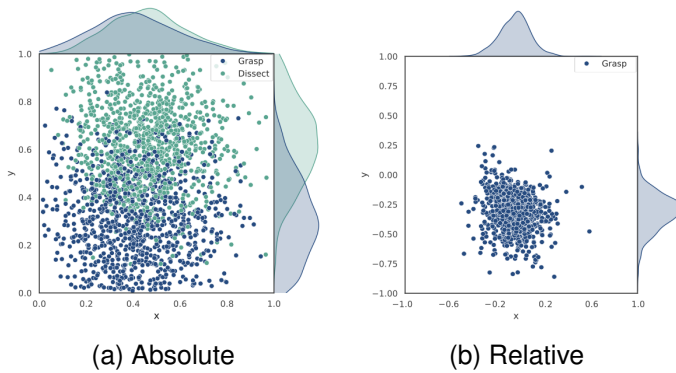


Fig. 7. Statistical distribution of grasping and dissection points in the dataset.

performance improvements, especially in out-of-distribution settings, such as with unseen procedures and surgeons. Beyond improving performance, attachment anchors provide transparent insight into how a robotic system could interpret grasping-relevant situations, supporting explainability and human oversight. Together, these findings establish attachment anchors as a meaningful step towards autonomous assistance in robotic surgery.

ACKNOWLEDGMENTS

This work has been funded by the Bavarian Collaborative Research Program (BayVFP) under der Funding Line Digitization. Grant number: DIK-2406-0025.

REFERENCES

- [1] J. Ahmed, M. A. Kuzu, N. Figueiredo, J. Khan, and A. Parvaiz, "Three-step standardized approach for complete mobilization of the splenic flexure during robotic rectal cancer surgery," *Colorectal Disease*, vol. 18, no. 5, pp. O171–O174, May 2016.
- [2] T. Haidegger, "Autonomy for surgical robots: Concepts and paradigms," *IEEE Transactions on Medical Robotics and Bionics*, vol. 1, no. 2, pp. 65–76, 2019.
- [3] J. N. K. Wah, "The rise of robotics and ai-assisted surgery in modern healthcare," *Journal of Robotic Surgery*, vol. 19, no. 1, p. 311, Jun. 2025.
- [4] R. Younis, A. Yamlahi, S. Bodenstedt, P. Scheickl, A. Kisilenko, M. Daum, A. Schulze, P. A. Wise, F. Nickel, F. Mathis-Ullrich, L. Maier-Hein, B. P. Müller-Stich, S. Speidel, M. Distler, J. Weitz, and M. Wagner, "A surgical activity model of laparoscopic cholecystectomy for co-operation with collaborative robots," *Surgical Endoscopy*, 2024.
- [5] C. Kunz, M. Kraus, R. Younis, M. Wagner, and F. Mathis-Ullrich, "Statistical shape models for grasp point determination in laparoscopic surgeries," *Current Directions in Biomedical Engineering*, vol. 10, no. 1, pp. 41–44, 2024.
- [6] J. W. B. Kim, J.-T. Chen, P. Hansen, L. X. Shi, A. Goldenberg, S. Schmidgall, P. M. Scheickl, A. Deguet, B. M. White, D. R. Tsai, R. J. Cha, J. Jopling, C. Finn, and A. Krieger, "Srt-h: A hierarchical framework for autonomous surgery via language-conditioned imitation learning," *Science Robotics*, vol. 10, no. 104, 2025.
- [7] Y. Kassahun, B. Yu, A. Tibebu, D. Stoyanov, S. Giannarou, J. Metzen, and E. Vander Poorten, "Surgical robotics beyond enhanced dexterity instrumentation: a survey of machine learning techniques and their role in intelligent and autonomous surgical actions," *International journal of computer assisted radiology and surgery*, vol. 11, 10 2015.
- [8] E. M. Burns, A. Bottle, P. Aylin, A. Darzi, R. J. Nicholls, and O. Faiz, "Variation in reoperation after colorectal surgery in england as an indicator of surgical performance: retrospective analysis of hospital episode statistics," *BMJ*, vol. 343, p. d4836, Aug. 2011.
- [9] M. A. Daghmouri, M. A. Chaouch, M. Oueslati, L. Rebai, and H. Oweira, "Regional techniques for pain management following laparoscopic elective colonic resection: A systematic review," *Annals of Medicine and Surgery*, vol. 72, p. 103124, 2021.
- [10] Z. Yin and Y. Li, "Overview of robotic grasp detection from 2d to 3d," *Cognitive Robotics*, vol. 2, pp. 73–82, 2022.
- [11] K. Park, T. Patten, and M. Vincze, "Pix2pose: Pixel-wise coordinate regression of objects for 6d pose estimation," *CoRR*, 2019.
- [12] D. Morrison, P. Corke, and J. Leitner, "Learning robust, real-time, reactive robotic grasping," *The International Journal of Robotics Research*, vol. 39, no. 2-3, pp. 183–201, 2020.
- [13] H.-S. Fang, C. Wang, H. Fang, M. Gou, J. Liu, H. Yan, W. Liu, Y. Xie, and C. Lu, "Anygrasp: Robust and efficient grasp perception in spatial and temporal domains," 2023.
- [14] Z. Xie, X. Liang, and C. Roberto, "Learning-based robotic grasping: A review," *Frontiers in Robotics and AI*, vol. Volume 10 - 2023, 2023.
- [15] B. Rosa, C. Gruijthuisen, B. Van Cleynenbreugel, J. Vander Sloten, D. Reynaerts, and E. Vander Poorten, "Estimation of optimal pivot point for remote center of motion alignment in surgery," *International journal of computer assisted radiology and surgery*, vol. 10, 05 2014.
- [16] P. K. Kanithi, C. Christophe, M. A. Pimentel, T. Raha, N. Saadi, H. Javed, S. Maslenkova, N. Hayat, R. Rajan, and S. Khan, "Medic: Towards a comprehensive framework for evaluating llms in clinical applications," 2024.
- [17] A. Attanasio, B. Scaglioni, M. Leonetti, A. F. Frangi, W. Cross, C. S. Biyani, and P. Valdastrì, "Autonomous tissue retraction in robotic assisted minimally invasive surgery – a feasibility study," *IEEE Robotics and Automation Letters*, vol. 5, no. 4, pp. 6528–6535, 2020.
- [18] N. Uday Shinde, X. Liang, F. Liu, Y. Zhang, F. Richter, S. Herbert, and M. C. Yip, "JIGGLE: An Active Sensing Framework for Boundary Parameters Estimation in Deformable Surgical Environments," *arXiv e-prints*, May 2024.
- [19] C.-P. Wang, C. Chen, X. Liang, S. Atar, F. Richter, and M. Yip, "Feedback matters: Augmenting autonomous dissection with visual and topological feedback," 2025.
- [20] E. Tagliabue, D. Dall'Alba, M. Pfeiffer, M. Piccinelli, R. Marin, U. Castellani, S. Speidel, and P. Fiorini, "Data-driven intra-operative estimation of anatomical attachments for autonomous tissue dissection," *IEEE Robotics and Automation Letters*, vol. 6, no. 2, pp. 1856–1863, 2021.
- [21] D. Meli, E. Tagliabue, D. Dall'Alba, and P. Fiorini, "Autonomous tissue retraction with a biomechanically informed logic based framework," *CoRR*, vol. abs/2109.02316, 2021.
- [22] L. Maier-Hein, M. Eisenmann, D. Sarikaya, K. März, T. Collins, A. Malpani, J. Fallert, H. Feussner, S. Giannarou, P. Mascagni, H. Nakawala, A. Park, C. Pugh, D. Stoyanov, S. S. Vedula, K. Cleary, G. Fichtinger, G. Forestier, B. Gibaud, T. Grantcharov, M. Hashizume, D. Heckmann-Nötzel, H. G. Kenngott, R. Kikinis, L. Mündermann, N. Navab, S. Onogur, T. Roß, R. Sznitman, R. H. Taylor, M. D. Tizabi, M. Wagner, G. D. Hager, T. Neumuth, N. Padoy, J. Collins, I. Gockel, J. Goedeke, D. A. Hashimoto, L. Joyeux, K. Lam, D. R. Leff, A. Madani, H. J. Marcus, O. Meireles, A. Seitel, D. Teber, F. Ückert, B. P. Müller-Stich, P. Jannin, and S. Speidel, "Surgical data science – from concepts toward clinical translation," *Medical Image Analysis*, vol. 76, p. 102306, 2022.
- [23] F. R. Kolbinger, S. Bodenstedt, M. Carstens, S. Leger, S. Krell, F. M. Rinner, T. P. Nielen, J. Kirchberg, J. Fritzmann, J. Weitz, M. Distler, and S. Speidel, "Artificial intelligence for context-aware surgical guidance in complex robot-assisted oncological procedures: An exploratory feasibility study," *European Journal of Surgical Oncology*, vol. 50, no. 12, p. 106996, 2024.
- [24] J. Redmon, S. Divvala, R. Girshick, and A. Farhadi, "You only look once: Unified, real-time object detection," 2016.
- [25] A. Howard, M. Sandler, G. Chu, L. Chen, B. Chen, M. Tan, W. Wang, Y. Zhu, R. Pang, V. Vasudevan, Q. V. Le, and H. Adam, "Searching for mobilenetv3," *CoRR*, vol. abs/1905.02244, 2019.
- [26] A. van den Oord, Y. Li, and O. Vinyals, "Representation learning with contrastive predictive coding," *CoRR*, vol. abs/1807.03748, 2018.